Atmos. Chem. Phys., 21, 15221–15237, 2021
https://doi.org/10.5194/acp-21-15221-2021

Atmospheric Chemistry and Physics
Open Access
EGU

Formation and evolution of secondary organic aerosols derived from urban-lifestyle sources: vehicle exhaust and cooking emissions

Zirui Zhang[1,★], Wenfei Zhu[1,★], Min Hu[1,2,5], Kefan Liu[1], Hui Wang[1], Rongzhi Tang[1], Ruizhe Shen[1], Ying Yu[1], Rui Tan[1], Kai Song[1], Yuanju Li[1], Wenbin Zhang[3], Zhou Zhang[3], Hongming Xu[3], Shijin Shuai[3], Shuangde Li[4], Yunfa Chen[4], Jiayun Li[6], Yuesi Wang[6], and Song Guo[1]

[1]State Key Joint Laboratory of Environmental Simulation and Pollution Control, International Joint Laboratory for Regional Pollution Control, Ministry of Education (IJRC), College of Environmental Sciences and Engineering, Peking University, Beijing 100871, China
[2]Collaborative Innovation Center of Atmospheric Environment and Equipment Technology, Nanjing University of Information Science & Technology, Nanjing 210044, China
[3]State Key Laboratory of Automotive Safety and Energy, Tsinghua University, Beijing 100084, China
[4]State Key Laboratory of Multiphase Complex Systems, Institute of Process Engineering, Chinese Academy of Sciences, Beijing 100190, China
[5]Beijing Innovation Center for Engineering Sciences and Advanced Technology, Peking University, Beijing 100871, China
[6]State Key Laboratory of Atmospheric Boundary Layer Physics and Atmospheric Chemistry (LAPC), Institute of Atmospheric Physics, Chinese Academy of Sciences, Beijing 100029, China
★These authors contributed equally to this work.

Correspondence: Min Hu (minhu@pku.edu.cn)

Received: 11 January 2021 – Discussion started: 22 February 2021
Revised: 9 September 2021 – Accepted: 13 September 2021 – Published: 13 October 2021

Abstract. Vehicle exhaust and cooking emissions are closely related to the daily life of city dwellers. Here, we defined the secondary organic aerosols (SOAs) derived from vehicle exhaust and cooking emissions as "urban-lifestyle SOAs" and simulated their formation using a Gothenburg potential aerosol mass reactor (Go:PAM). The vehicle exhaust and cooking emissions were separately simulated, and their samples were defined as "vehicle group" and "cooking group", respectively. After samples had been aged under 0.3–5.5 d of equivalent photochemical age, these two urban-lifestyle SOAs showed markedly distinct features in the SOA mass growth potential, oxidation pathways, and mass spectra. The SOA/POA (primary organic aerosol) mass ratios of vehicle groups (107) were 44 times larger than those of cooking groups (2.38) at about 2 d of equivalent photochemical age, according to the measurement of scanning mobility particle sizer (SMPS). A high-resolution time-of-flight aerosol mass spectrometer was used to perform a deeper analysis. It revealed that organics from the vehicle may undergo the alcohol and/or peroxide and carboxylic acid oxidation pathway to produce abundant less and more oxidized oxygenated OAs (LO-OOAs and MO-OOAs), and only a few primary hydrocarbon-like organic aerosols (HOAs) remain unaged. In contrast, organics from cooking may undergo the alcohol and/or peroxide oxidation pathway to produce moderate LO-OOAs, and comparable primary cooking organic aerosols (COAs) remain unaged. Our findings provide an insight into atmospheric contributions and chemical evolutions for urban-lifestyle SOAs, which could greatly influence the air quality and health risk assessments in urban areas.

Published by Copernicus Publications on behalf of the European Geosciences Union.

1 Introduction

Organic aerosols (OAs) contribute 20 %–90 % of submicron aerosols in mass (Jimenez et al., 2009; Zhang et al., 2011), and their fraction in urban areas is higher than that in suburban or background areas (Zhou et al., 2020). The OAs can be divided into primary organic aerosols (POAs) and secondary organic aerosols (SOAs). There are many potential sources of POAs, such as coal combustion, biomass burning, vehicle exhaust, cooking procedure, and so forth (Jimenez et al., 2009; Zhang et al., 2011; Zhou et al., 2020). SOAs are formed via the oxidation of gas-phase organics and the distribution between the gas and particle phase (Donahue et al., 2009). Significant SOA formation has been observed in several urban areas, but models typically fail to simulate this phenomenon accurately (Matsui et al., 2009; Kleinman et al., 2008; Volkamer et al., 2006; de Gouw et al., 2008). This discrepancy may be attributed to the limited knowledge of the sources and characteristics of urban SOAs.

Over the past decades, megacities have already become widespread in developed regions, and rapid urbanization has been sweeping across the globe especially in developing areas (Zhang et al., 2015). An increasing number of people tend to live in urban areas for their livelihood, where they suffer from serious air pollution typically simultaneously involving vehicle and cooking fumes (An et al., 2019; Zhang et al., 2015; Chan and Yao, 2008; Guo et al., 2014, 2020). For instance, polycyclic aromatic hydrocarbons (PAHs) are important carcinogens coming from vehicles and cooking, which can cause severe lung cancer (Seow et al., 2000; Kim et al., 2015; Zhong et al., 1999). After PAHs are emitted into ambient air, they can be oxidized, be distributed into the particle phase, and finally become part of POAs or SOAs, thus adding unknown deviations to health risk assessments (Masuda et al., 2020).

Vehicle and cooking emissions are important sources of OAs in urban areas (Rogge et al., 1991, 1993; Hu et al., 2015; Hallquist et al., 2016; Crippa et al., 2013; Mohr et al., 2012; Guo et al., 2013, 2012). Take the megacity (defined as a total metro area population of more than 3 million) for example, in London, where these two lifestyle sources contribute 50 % of OAs on average (Allan et al., 2010). In addition, vehicles themselves could even contribute 62 % of OA mass in the rush hour of New York City (Sun et al., 2012). As for OA source appointments in Paris, vehicle and cooking contribute a maximum of 46 %–50 % of OAs (Crippa et al., 2013). According to seasonal observations in Beijing, at least 30 % of OAs there come from vehicle and cooking emissions (Hu et al., 2017). Briefly, these two urban-lifestyle sources are closely related to the daily life of city residents and could account for 20 %–60 % of ambient OA mass in urban areas when only considering their contributions to POAs (Allan et al., 2010; Sun et al., 2011; Ge et al., 2012; Sun et al., 2012; Lee et al., 2015; Hu et al., 2017). Furthermore, it has been speculated that vehicle and cooking emissions might even contribute over 90 % of SOAs in downtown Los Angeles by applying hypothetical model parameters with a certain degree of uncertainty (Hayes et al., 2015). Therefore, vehicle and cooking are momentous sources of both POAs and SOAs in urban areas and could be defined as "urban-lifestyle sources of OAs".

As is well-known, large quantities of volatile, semi-volatile, and intermediate-volatility organic compounds (VOCs, SVOCs, and IVOCs, respectively) are emitted from vehicle and cooking sources, leading to large potential SOA production (Klein et al., 2016; Katragadda et al., 2010; Liu et al., 2017c; Tang et al., 2019; Zhao et al., 2015; Esmaeilirad and Hosseini, 2018; Zhao et al., 2017; Yu et al., 2020). Laboratory studies have investigated the formation of vehicle or cooking SOAs using a smog chamber or an oxidation flow reactor (OFR). On the one hand, some laboratory experiments have investigated the vehicle SOAs based on variables such as fuel types, engine types, operating conditions, and so on (Deng et al., 2020; Suarez-Bertoa et al., 2015; Zhao et al., 2015; Du et al., 2018). Several smog chamber studies have found that the mass loading of SOAs exceeds that of POAs when the equivalent photochemical age is more than 1 d (Gordon et al., 2013; Chirico et al., 2010; Nordin et al., 2013). Besides, an OFR could simulate a higher OH exposure, and the peak SOA production occurs after 2–3 d of equivalent atmospheric oxidation (Tkacik et al., 2014; Zhao et al., 2018; Timonen et al., 2017; Watne et al., 2018; Alanen et al., 2017). The mass spectra of vehicle SOAs has shown both semi-volatile and low-volatility oxygenated organic aerosol (SV-OOA and LV-OOA) features along with the growth of oxidation degree (Tkacik et al., 2014). NO_x levels may greatly influence the chemical evolution of vehicle SOAs, and their NO_x and VOC values are often strongly dependent on the sampling time and place in urban areas (Zhan et al., 2021; Wei et al., 2014). It has been found that the photochemical ages for maximum SOA production under high-NO_x levels are lower than those under low-NO_x levels among OFR simulations (Liao et al., 2021). On the other hand, only a few laboratory experiments have investigated the cooking SOAs based on simplified ingredients or a single cooking method, involving heated cooking oils (Liu et al., 2017a, 2018), stir-frying spices (Liu et al., 2017b), charbroiled meat (Kaltsonoudis et al., 2017), and Chinese cuisines (Z. Zhang et al., 2020). These laboratory experiments have indicated that the characteristics of SOAs are influenced by multiple factors, such as cooking methods, fuels, cookers, or ingredients. The mass ratios of POAs and SOAs derived from cooking are comparable, and the mass spectra of SOAs show many more similarities with the ambient semi-volatile oxygenated OA (SV-OOA) factors (Liu et al., 2018). Although these laboratory studies have provided important insights into the secondary formation of vehicle and cooking SOAs, significant uncertainties still exist. Nobody has compared the different natures generated from these two

urban-lifestyle sources in detail, let alone pointed out their potentially different roles in the real atmosphere.

In this work, we have designed our vehicle and cooking laboratory experiments according to daily basis situations in urban areas of China. For vehicle exhaust simulation, China Phase V gasoline and three common operating conditions were chosen. For cooking emissions simulation, four prevalent Chinese domestic cooking types were evaluated. A Gothenburg potential aerosol mass reactor (Go:PAM) was used as the oxidation system. All the fresh or aged OAs were characterized in terms of the mass growth potential, elemental ratios, oxidation pathways, and mass spectra. The aged OAs could be divided into POAs and SOAs. The latter was defined as "urban-lifestyle SOAs" whose mass spectra would be compared with those of ambient SOAs, like less oxidized oxygenated OAs (LO-OOAs) and more oxidized oxygenated OAs (MO-OOAs) measured in urban areas of China. These findings aim to support the estimation of these two urban-lifestyle SOAs in ambient air, informing the policy formulation of pollution source control and the health risk assessment of exposure to vehicle and cooking fumes.

2 Materials and method

2.1 Experimental setup

The vehicle experiment was conducted from July to October in 2019 at the Department of Automotive Engineering, Tsinghua University. The cooking experiment was conducted from November 2019 to January 2020 at Langfang Branch, Institute of Process Engineering, Chinese Academy of Sciences. The laboratory simulations of the two urban-lifestyle SOAs were conducted with the same oxidation and measurement system. Tables 1–2 contain information on vehicle and cooking experiment conditions. The vehicle exhaust was emitted from a gasoline direct injection (GDI) engine with China V gasoline (similar to Euro 5) under three speeds ($20, 40, 60\,\mathrm{km\,h^{-1}}$), which represented the urban road conditions in China (Zhang et al., 2020a). The commercial China Phase V gasoline was used as the fuel, which has an equivalent octane number 92 level (RON 92), 10 ppm (v/v, max) sulfur, 25 % (v/v, max) olefin, about 40 % (v/v, max) aromatics, $2\,\mathrm{mg\,L^{-1}}$ of Mn, and no oxygenates (Yinhui et al., 2016). More information about the GDI engine can be found in Tables S2–S3 in the Supplement. For all experiments, the GDI engine ran in a single room; its exhaust was drawn into the pipeline and then entered Go:PAM at a 30-fold dilution where aerosols and gases reacted at a stable temperature and relative humidity. On the other hand, four kinds of domestic cuisines were cooked with liquefied petroleum gas (LPG) in an iron wok, including deep-frying chicken; shallow-frying tofu; stir-frying cabbage; and Kung Pao chicken composed of cucumbers, peanuts, and chicken. The cooking time and oil temperature were different due to the inherent features of the ingredients. For all experiments, the closed kitchen was full of fumes where the vision was blurred and the air was choky after the long time taken for the cooking process. Subsequently, the cooking fumes were drawn into a pipeline from the kitchen to a lab and then entered Go:PAM at an 8-fold dilution where aerosols and gases reacted at a stable temperature and relative humidity. Both vehicle and cooking fumes were diluted at a constant ratio by a Dekati diluter (eDiluter, Dekati Ltd.). Vehicle exhaust from a tailpipe was first diluted by a gradient-heated dilution system (6-fold) and then diluted by an unheated dilution system (5-fold). The temperature of sample flow was near the indoor temperature (20–25 °C) after secondary dilution systems. The cooking fumes were collected through the kitchen ventilator, where the temperature was similar to that of indoor air. Go:PAM was able to produce high OH exposures using an ultraviolet lamp ($\lambda = 254\,\mathrm{nm}$) in the presence of ozone and water vapor to simulate the photochemical oxidation in the atmosphere (J. Li et al., 2019; Watne et al., 2018). The internal structure of Go:PAM can be found in Fig. S1. Blank experiments were separately designed in the presence of boiling water or dilution air under the same condition. The OA concentrations of blank groups were far below those of experimental groups, which indicated the background values were minor (Table S1 in the Supplement). All the sampling tubes were made of silanized stainless steel which is appropriate for simultaneous gas and particle sampling (Deming et al., 2019; Wiedensohler et al., 2012). More details about the experimental design and instruments can be found in the Supplement.

2.2 Measurements of the gas and particle phase

Figure 1 presents the design of this laboratory simulation. The gases and aerosols were emitted from the GDI room or kitchen and then reacted and sampled in a lab. The chemical compositions of OAs were measured by a high-resolution time-of-flight aerosol mass spectrometer (HR-ToF-AMS, Aerodyne Research Inc.), in which the non-refractory particles including organics, sulfate, nitrate, ammonium, and chloride were instantly vaporized by a 600 °C tungsten filament. Next, the vaporized compounds were ionized by electron impact (EI) ionization with 70 eV. Finally, the fragment ions were pulsed to a time-of-flight mass spectrometry (MS) chamber and detected by the multi-channel plate detector (MCP). More information about the HR-ToF-AMS is described in detail elsewhere (Nash et al., 2006; DeCarlo et al., 2006). In this study, its time resolution was 2 min (precisely, 1 min for a mass-sensitive V mode and 1 min for a high-mass-resolution W mode). As for the HR-ToF-AMS, the aged OAs were those measured under certain OH exposure. Two sets of scanning mobility particle sizers (SMPS-1, differential mobility analyzer, Electrostatic Classifier model 3080; condensation particle counter model 3778; SMPS-2, differential mobility analyzer, Electrostatic Classi-

Table 1. Descriptions of vehicle exhaust and sampling procedures.

Experiment	Revolving speed	Torque	Sampling time	Parallels	Particle density	Fuel	Sampling line temperature
GDI 20 km h^{-1}	1500 Hz	16 N m	60 min	3–5	1.1–1.2 g cm^{-3}	Gasoline (China V, similar to Euro 5)	20–25 °C
GDI 40 km h^{-1}	2000 Hz	16 N m	70 min	3–6			
GDI 60 km h^{-1}	1750 Hz	32 N m	60 min	3–5			

fier model 3082; condensation particle counter model 3772; TSI Inc.) scanned individually every 2 min before and after Go:PAM to identify the size distribution and number concentration of particles. The SMPS-1 determined the mass concentration of POAs, while the SMPS-2 determined the mass concentration of aged OAs, and their mass difference could be regarded as the SOAs. A SO_2 analyzer (model 43i, Thermo Electron Corp.) was used to measure the decay of SO_2 in offline adjustment. The measured CO_2 concentrations (model 410i, Thermo Electron Corp.) were used to conduct CO_2 correction for AMS data to reduce the CO_2 interference on organic fragments in mass spectra of the HR-ToF-AMS. The particle densities were measured through the determination of the DMA–CPMA–CPC system (DMA – differential mobility analyzer, Electrostatic Classifier model 3080, TSI Inc.; CPMA – centrifugal particle mass analyzer, version 1.53, Cambustion Ltd.; CPC – condensation particle counter, model 3778, TSI Inc.). To prevent freshly warm gas from condensing on the pipe wall, sampling pipes were equipped with heat insulation cotton and a temperature controller. Silicon tubes were used to dry the emissions before they entered measuring instruments. Before each experiment, all pipelines and the Go:PAM chamber were continuously flushed with purified dry air, until the concentrations were minimal (just like blank groups in Table S1) when the UV was on or off. The SOAs formed in each experiment represented the upper limit due to the presence of background concentration.

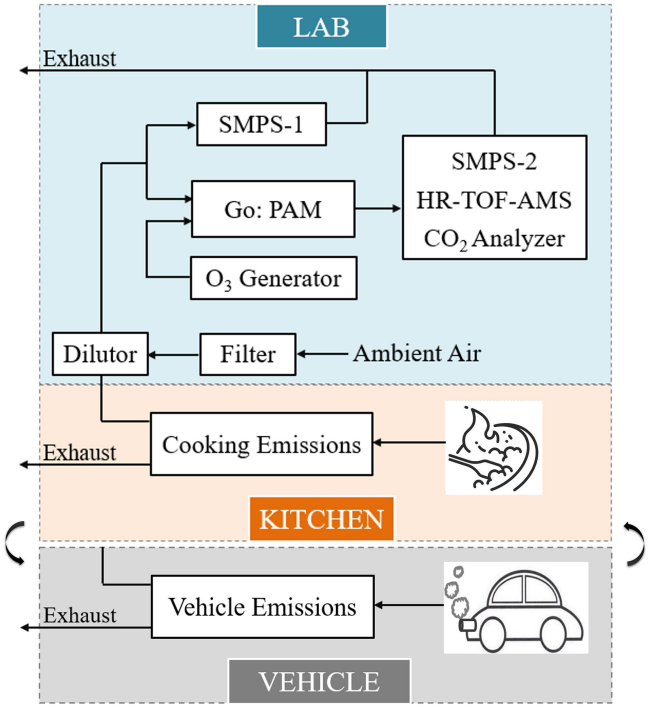

Figure 1. Schematic of experiment system.

2.3 Data analysis

2.3.1 HR-ToF-AMS data

The SQUIRREL 1.57 and PIKA 1.16 packages written in Igor (WaveMetrics Incorporation, USA) were used to analyze the HR-ToF-AMS data including mass concentrations, elemental ratios, ion fragments, and mass spectra. The ionization efficiency (IE), relative ionization efficiency (RIE), and collection efficiency (CE) were determined individually before data processing. The 300 nm ammonium nitrate particles were applied for converting the instrument signals to actual mass concentrations (Jayne et al., 2000; Drewnick et al., 2005). Before the formal experiment, the IE and RIE_{SO_4} were calculated by the comparison of the HR-ToF-AMS and SMPSs, when the sampling flow was generated by 300 nm ammonium nitrate and 300 nm ammonium sulfate, respectively, with an aerosol generator (DMT Inc.). The CE was a fluctuant value influenced by the emission condition, so it was estimated by the comparison of the HR-ToF-AMS (sampling after Go:PAM) and SMPS-2 (sampling after Go:PAM) during the formal experiment. The CE and RIE_{Org} were theoretically different in every emission or oxidation condition, so we directly used the SMPS measurements to determine the aged OA mass concentration. As for the cooking experiment, the IE value was 7.77×10^{-8}, the RIE_{SO_4} was 1.4, the RIE_{Org} was 1.4 (default value, the fluctuation in RIE_{Org} was included in the CE), and the average CE was about 0.55 (ranged from 0.3 to 0.7). As for the vehicle experiment, the IE value was 7.69×10^{-8}, the RIE_{SO_4} was 1.3, the RIE_{Org} was 1.4 (default value, the fluctuation in RIE_{Org} was included in the CE), and the average CE was about 0.6 (ranged from 0.4 to 0.7). For some of the experimental groups, the mass spectra were resolved by positive matrix factorization (PMF) analysis to perform deeper analyses (Ulbrich et al., 2009).

Table 2. Descriptions of cooking emissions and sampling procedures.

Experiment	Cooking material	Oil temperature	Total cooking time	Number of dishes	Sampling time	Parallels	Particle density	Fuel and cookware	Kitchen volume	Sampling line temperature
Deep-fried meat	170 g chicken, 500 mL corn oil, and a few condiments	145–155 °C	66 min	5	90 min	3–8	1.11 ± 0.02 g cm^{-3}	Liquefied petroleum gas (LPG) and iron wok	78 m^3 (5.6 m × 4 m × 3.5 m)	20–25 °C
Shallow-fried tofu	500 g tofu, 200 mL corn oil, and a few condiments	100–110 °C	64 min	5	60 min	3–5	1.04 ± 0.03 g cm^{-3}			
Stir-fried cabbage	300 g cabbage, 40 mL corn oil, and a few condiments	95–105 °C	47 min	5	58 min	3–5	1.16 ± 0.03 g cm^{-3}			
Kung Pao chicken	150 g chicken, 50 g peanut, 50 g cucumber, 40 mL corn oil, and a few condiments	Unmeasured*	40 min	5	60 min	3–5	1.07 ± 0.02 g cm^{-3}			

* It needed to be stirred constantly, so the oil temperature was unstable.

2.3.2 Determination and evaluation of oxidation conditions in Go:PAM

The Go:PAM conditions for vehicle and cooking experiments could be seen in Tables 3 and 4, respectively. Their experiment conditions (such as residence time and RH) were not completely the same because of the inherent difference between the two sources and their experimental design, whereas some comparisons could still be analyzed under a similar OH exposure, and their RH conditions were both low where photochemical oxidations instead of aqueous-phase processing dominated the chemical evolution process (Xu et al., 2017). The OH exposures and corresponding photochemical ages in Go:PAM were calculated through an offline adjustment based on the decay of SO_2 (Lambe et al., 2011). As shown in Eq. (1), K_{OH-SO_2} is the reaction rate constant of the OH radical and SO_2 (9.0×10^{-13} molec.$^{-1}$ cm^3 s^{-1}). $SO_{2,f}$ and $SO_{2,i}$ are the SO_2 concentrations (ppb) under the conditions of the UV lamp being on or off, respectively. The photochemical age (days) can be calculated in Eq. (2) when assuming the OH concentration is 1.5×10^6 molecules cm^{-3} in the atmosphere (Mao et al., 2009).

$$\text{OH exposure} = \frac{-1}{K_{OH-SO_2}} \times \ln\left(\frac{SO_{2,f}}{SO_{2,i}}\right) \quad (1)$$

$$\text{Photochemical age} = \frac{\text{OH exposure}}{24 \times 3600 \times 1.5 \times 10^6} \quad (2)$$

Except for in the offline calibration based on the decay of SO_2, a flow reactor exposure estimator was also used in this study (Peng et al., 2016). The OH exposures calculated by these two methods showed a good correlation (Figs. S2 and S3). This estimator could also evaluate the potential non-OH reactions in the flow reactor such as the photolysis of VOCs and the reactions with $O(^1D)$, $O(^3P)$, and O_3. The flow reactor exposure estimator showed that OH reactions played a dominant role in our experiments. It was found that the heterogeneous reaction of ozone with oleic acid aerosol particles was influenced by the humidity and reaction time in an aerosol flow reactor (Vesna et al., 2009). Therefore, non-OH reactions which were not included in specific designs in our experiment, such as the ozonolysis of unsaturated fatty acids, may also be important in forming SOAs.

Furthermore, both the external OH reactivity and the OH exposure were influenced by external OH reactants, such as NO_x and VOCs, during experiments. The NO_x concentration was measured by a NO–NO_2–NO_x analyzer (model 42i, Thermo Electron Corp., USA). As for VOCs, we have divided them into five types including alkane, alkene, aromatic, O-VOCs (oxidized VOCs, mainly including aldehyde and ketone), and X-VOCs (halogenated VOCs) using the measurement of GC-MS (gas chromatography–mass spectrometry, GC 7890, MS 5977, Agilent Technologies Inc.). The compounds with relatively high proportions were regarded as surrogate species for each type of VOC. The total concentrations of VOCs were determined by a portable TVOC analyzer

https://doi.org/10.5194/acp-21-15221-2021

Table 3. The Go:PAM conditions for vehicle experiments.

Experiment	O_3 concentration (ppbV)	OH exposure[a] ($\times 10^{10}$ molecules cm^{-3} s)	Photochemical age (days, $[OH] = 1.5 \times 10^6$ molecules cm^{-3})	External OH reactivity of SO_2 during offline calibration (s^{-1})	External OH reactivity of VOCs during experiment (s^{-1})	Ratio of OH Exposure calculated by an estimator[b] to that calculated by the decay of SO_2[a]	Temperature and RH in Go : PAM	Basic description of Go:PAM	Wall Loss
GDI 20 km h^{-1}	624	7.79	0.6	15.8	10.4	119 %	Temp: 19–22 °C. RH: 44 %–49 %	Volume: 7.9 L. Flow rate: 4 L min^{-1} for sample air and 1 L min^{-1} for sheath gas. Residence time: 110 s.	The wall loss of particles was adjusted in each size bin measured by two synchronous SMPSs (two SMPSs run before and after Go:PAM, respectively). The wall loss of the gas phase is minor according to previous research.
	2367	21.4	1.7						
	4433	37.4	2.9						
	6533	53.8	4.2						
	8050	65.6	5.1						
	8701	70.6	5.5						
GDI 40 km h^{-1}	The same as the 20 km h^{-1} experiments				20.2	83 %			
GDI 60 km h^{-1}	The same as the 20 km h^{-1} experiments				16.7	94 %			

[a] OH exposure was calculated based on the decay of SO_2. [b] OH exposure for each ingredient was calculated based on the OFR estimator.

Table 4. The Go:PAM conditions for cooking experiments.

Experiment	O_3 concentration (ppbV)	OH exposure[a] ($\times 10^{10}$ molecules cm^{-3} s)	Photochemical age (days, $[OH] = 1.5 \times 10^6$ molecules cm^{-3})	External OH reactivity of SO_2 during offline calibration (s^{-1})	External OH reactivity of VOCs during experiment (s^{-1})	Ratio of OH exposure calculated by an estimator[b] to that calculated by the decay of SO_2[a]	Temperature and RH in Go : PAM	Basic description of Go:PAM	Wall loss
Deep-fried chicken	–	0	0.0	24.0	25.7	97 %	Temp: 16–19 °C. RH: 18 %–23 %	Volume: 7.9 L. Flow rate: 7 L min^{-1} for sample air and 3 L min^{-1} for sheath gas. Residence time: 55 s.	The wall loss of particles was adjusted in each size bin measured by two synchronous SMPSs (two SMPSs run before and after Go:PAM, respectively). The wall loss of the gas phase is minor according to previous research.
	310	4.3	0.3						
	1183	9.6	0.7						
	2217	14.4	1.1						
	3267	21.4	1.7						
	4025	27.1	2.1						
Shallow-fried tofu	The same as the meat experiments				21.7	111 %			
Stir-fried cabbage	The same as the meat experiments				23.3	104 %			
Kung Pao chicken	The same as the meat experiments				23.6	103 %			

[a] OH exposure was calculated based on the decay of SO_2. [b] OH exposure for each ingredient was calculated based on the OFR estimator.

(PGM-7340, RAE Systems). The external OH reactivities for different vehicle experiments (10.4–20.2 s^{-1}) were all comparable to those of offline calibration results (15.8 s^{-1}), and the external OH reactivities for different cooking experiments (21.7–25.7 s^{-1}) were also comparable to that of offline calibration results (24.0 s^{-1}). Besides, the ratio of OH exposure calculated by the estimator to that calculated by the decay of SO_2 ranged from 83 % to 119 % for vehicle experiments and 97 % to 111 % for cooking experiments, which means that our offline OH exposure could be a representative value for all experiments. Detailed tests about mixing conditions and the wall loss of Go:PAM have been conducted in the previous work of J. Li et al. (2019) and Watne et al. (2018) and can be found in Fig. S4. In this study, we still corrected the wall loss of particles in each size bin measured by two synchronous SMPSs (two SMPSs run before and after Go:PAM, respectively). More details about Go:PAM can be found in the Supplement.

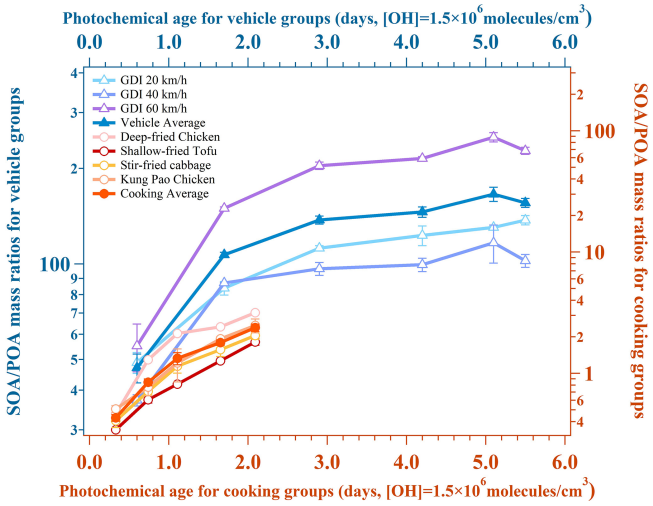

Figure 2. Secondary mass growth potential for two urban-lifestyle SOAs. The SMPS-1 determined the mass concentration of POAs, while the SMPS-2 determined the mass concentration of aged OAs, and their mass difference could be regarded as the SOAs. The average data and standard deviation bars are shown in the figure.

3 Results and discussion

3.1 Secondary formation potential of the urban-lifestyle OAs

The simulated SOAs could be generated by the photochemical oxidation from gaseous precursors and the heterogeneous oxidation from POAs. As Fig. 2 shows, the mass growth potential of the two urban-lifestyle OAs was quite different. The mass growth potential was represented by SOA/POA mass ratios. The SMPS-1 determined the mass concentration of POAs, while the SMPS-2 determined the mass concentration of aged OAs, and their mass difference could be regarded as the SOAs. Both their SOA/POA mass ratios increased gradually and finally reached the peak after 2–3 d of equivalent photochemical age, and the overall SOA mass growth potential of vehicle SOAs was far larger than that of cooking SOAs. When the equivalent photochemical age was near 2 d (1.7 d), the mass growth potential of vehicle SOAs ranged from 83 to 150. In contrast, the mass growth potential of cooking SOAs only ranged from 1.8 to 3.2 at about 2.1 d. Even though there was still a slight growth trend for cooking SOAs at the highest OH exposure, it exhibited a much weaker mass growth potential on the whole compared with that of vehicle SOAs. This significant distinction indicated that the vehicle exhaust may contribute abundant SOAs and relatively fewer POAs, while cooking emissions may produce moderate POAs and SOAs in the atmosphere, which could be attributed to their different types of gaseous precursors. Interestingly, a similar phenomenon has been observed from an OFR simulation at the urban roadside of Hong Kong, where potential SOAs from motor vehicle exhaust were much larger than primary hydrocarbon-like organic aerosols (HOAs), while potential SOAs from cooking emissions was comparable to primary cooking organic aerosols (COAs) (Liu et al., 2019).

3.2 Secondary formation pathway of the urban-lifestyle OAs

As Fig. 3 shows, the evolution of O : C molar ratios (O/C) of the two urban-lifestyle OAs was quite different. Although their oxidation degrees both increased gradually and finally reached the peak after 2–3 d of equivalent photochemical age, the O/C values of aged vehicle OAs were far larger than those of aged cooking OAs. When the equivalent photochemical age was 0.6 d, the O/C of aged vehicle OAs was 0.4–0.5, resembling a kind of LO-OOA in ambient air. When the equivalent photochemical age was near 2 d (1.7 d), the O/C of aged vehicle OAs could reach 0.6, which was almost like a type of MO-OOA in the atmosphere. In contrast, the O/C of aged cooking OAs only rose to 0.4 at 2.1 d, similarly to a kind of LO-OOA. These distinct features of O/C suggested that aged vehicle OAs were divided into LO-OOAs and MO-OOAs under different oxidation conditions, while the aged cooking OAs were composed of only LO-OOAs. This difference was probably related to their precursors.

Figure 4 illustrates diverse oxidation pathways of various sources of OA in a Van Krevelen diagram (Heald et al., 2010; Ng et al., 2011; Presto et al., 2014). The cooking groups fell along a line with a slope of −0.10 implying an alcohol and/or peroxide pathway in forming SOAs, while the vehicle groups fell along a line with a slope of −0.55 implying an oxidation pathway between alcohol and/or peroxide and carboxylic acid reaction. Additionally, these two secondary evolution properties are both different from those of biomass

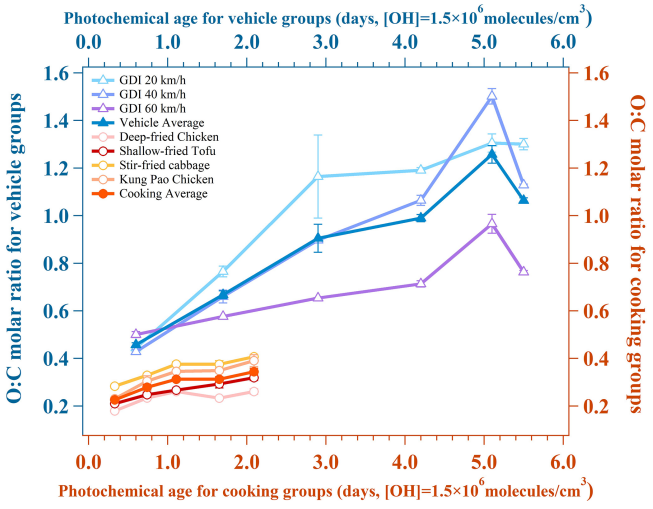

Figure 3. Evolution of O : C molar ratio for two urban-lifestyle OAs. The O : C molar ratios are determined by an HR-ToF-AMS. The average data and standard deviation bars at each gradient are shown in the figure.

burning OAs (slope ≈ -0.6) (Lim et al., 2019) and ambient OAs (slope ≈ -1 to -0.5) (Heald et al., 2010; Hu et al., 2017; Ng et al., 2011), indicating that these two urban-lifestyles SOAs may undergo distinct oxidation pathways.

3.3 Characteristics in mass spectra of the urban-lifestyle OAs

As shown in Fig. 5, the signal fraction of organic fragments at m/z 43 (f_{43}) and m/z 44 (f_{44}) has been widely adopted to represent the oxidation process of OAs (Ng et al., 2010; Hennigan et al., 2011). Generally, f_{43} and f_{44} derive from oxygen-containing fragments, the former comes from less oxidized components while the latter comes from more oxidized ones. The datasets of vehicle and cooking groups fell in different regions and showed different variations in the plot. Almost all aged cooking OAs displayed relatively lower f_{44} and higher f_{43}, and both their f_{43} and their f_{44} increased slightly with the growing OH exposure, eventually becoming distributed in the LO-OOA region. In contrast, all aged vehicle OAs displayed moderate f_{43} and abundant f_{44}, and only their f_{44} showed an obvious souring with the growing OH exposure, initially being distributed in the LO-OOA region but finally spreading near the MO-OOA region. These distinct evolutions of oxygen-containing fragments for two urban-lifestyle OAs implied their intrinsic oxidation pathways and precursors.

Figure 6 and Table 5 depict mass spectra and prominent peaks of aged OAs from two urban-lifestyle sources which could be used to deduce their inherent properties (Zhang et al., 2005; Kaltsonoudis et al., 2017; Liu et al., 2018; Chirico et al., 2010; Nordin et al., 2013; Z. Zhang et al., 2020). The maximum SOA mass growth potential of aged cooking OAs only ranged from 1.9–3.2, implying a mixture of POAs and SOAs, so their mass spectra needed to be comprehensively resolved by PMF to separate the POAs and SOAs (precisely, a kind of LO-OOA). Generally, there is at least one POA and one SOA (factor 1 – POA, factor 2 – SOA). When three or more factors were set, it was found that elemental ratios or mass spectra of additional OA factors are quite similar to those of factor 1 or factor 2, which means that it was hard to find another new OA factor. Therefore, two OA factors were finally set, one for POAs and another for SOAs. As Figs. S5–S8 show, the SOA factors present a larger fraction of oxygen-containing fragments (especially in m/z 28, m/z 29, m/z 43, m/z 44) and higher O/C, which is significantly different from the POA factors., whereas the mass growth potential of aged vehicle OAs was extremely high, suggesting that they were fully oxidized and almost composed of SOAs. According to the O/C ratios, the vehicle SOAs under 0.6 d of photochemical age were defined as vehicle LO-OOAs, while those under 2.9 d were regarded as vehicle MO-OOAs.

For average vehicle LO-OOA mass spectra, the prominent peaks were m/z 43 ($f_{43} = 0.133 \pm 0.003$), m/z 44 ($f_{44} = 0.077 \pm 0.001$), m/z 29 ($f_{29} = 0.076 \pm 0.003$), m/z 28 ($f_{28} = 0.066 \pm 0.001$), 41 ($f_{41} = 0.051 \pm 0.005$), and m/z 55 ($f_{55} = 0.043 \pm 0.004$) dominated by $C_2H_3O^+$, $C_3H_7^+$, CO_2^+, CHO^+, $C_2H_5^+$, CO^+, $C_3H_5^+$, $C_3H_3O^+$, and $C_4H_7^+$, while the prominent peaks of average vehicle MO-OOAs were m/z 44 ($f_{44} = 0.146 \pm 0.060$), m/z 28 ($f_{28} = 0.134 \pm 0.062$), m/z 43 ($f_{43} = 0.117 \pm 0.033$), m/z 29 ($f_{29} = 0.071 \pm 0.014$), m/z 45 ($f_{45} = 0.032 \pm 0.007$), and m/z 27 ($f_{27} = 0.030 \pm 0.009$) dominated by CO_2^+, CO^+, $C_2H_3O^+$, CHO^+, $C_2H_5^+$, CHO_2^+, $C_2H_5O^+$, and $C_2H_3^+$. Compared with vehicle SOA mass spectra from other studies (Table 5), our average GDI SOAs (LO-OOAs and MO-OOAs) illustrated more abundances of oxygen-containing ions than those of gasoline SOAs and diesel SOAs simulated by a smog chamber with lower OH exposures (Chirico et al., 2010; Nordin et al., 2013).

For average cooking LO-OOAs, they was less oxidized than those from vehicle groups, whose prominent peaks were m/z 43 ($f_{43} = 0.097 \pm 0.008$), m/z 44 ($f_{44} = 0.065 \pm 0.010$), m/z 29 ($f_{29} = 0.065 \pm 0.013$), m/z 41 ($f_{41} = 0.058 \pm 0.008$), m/z 55 ($f_{55} = 0.056 \pm 0.006$), and m/z 28 ($f_{28} = 0.053 \pm 0.011$) dominated by $C_2H_3O^+$, $C_3H_7^+$, CO_2^+, CHO^+, $C_2H_5^+$, $C_3H_5^+$, $C_3H_3O^+$, $C_4H_7^+$, and CO^+. Compared with other cooking SOA mass spectra (Table 5), our average cooking LO-OOAs had similar peaks to heated oil SOAs but were different from the meat charbroiling SOAs which displayed much more hydrocarbon-like features (Liu et al., 2018; Kaltsonoudis et al., 2017).

3.4 Potential chemical evolution of urban-lifestyle OAs in the atmosphere

The AMS mass spectra indicated that the chemical evolution of urban-lifestyle OAs in Go:PAM might provide new

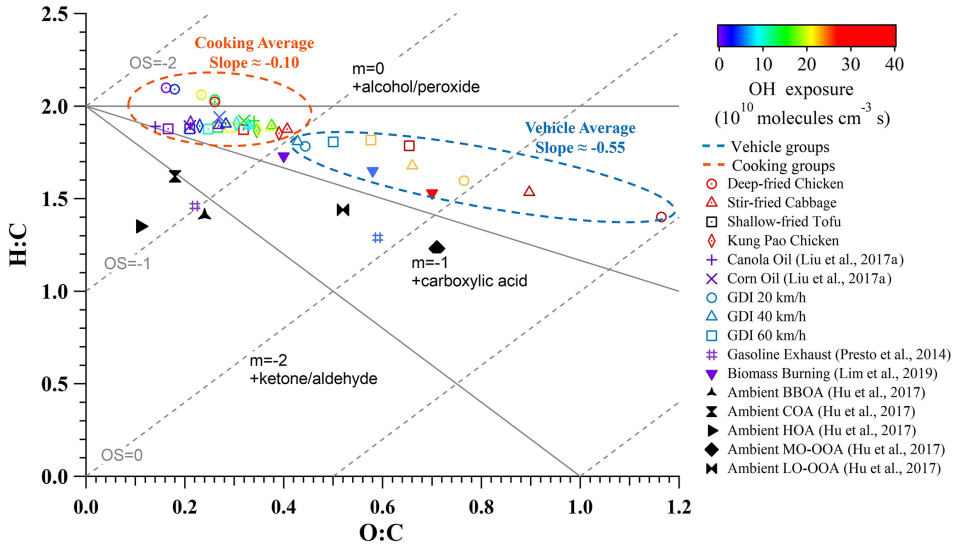

Figure 4. Van Krevelen diagram of OAs from various sources. O : C and H : C are determined by an HR-ToF-AMS. The average data at each gradient are shown in the figure.

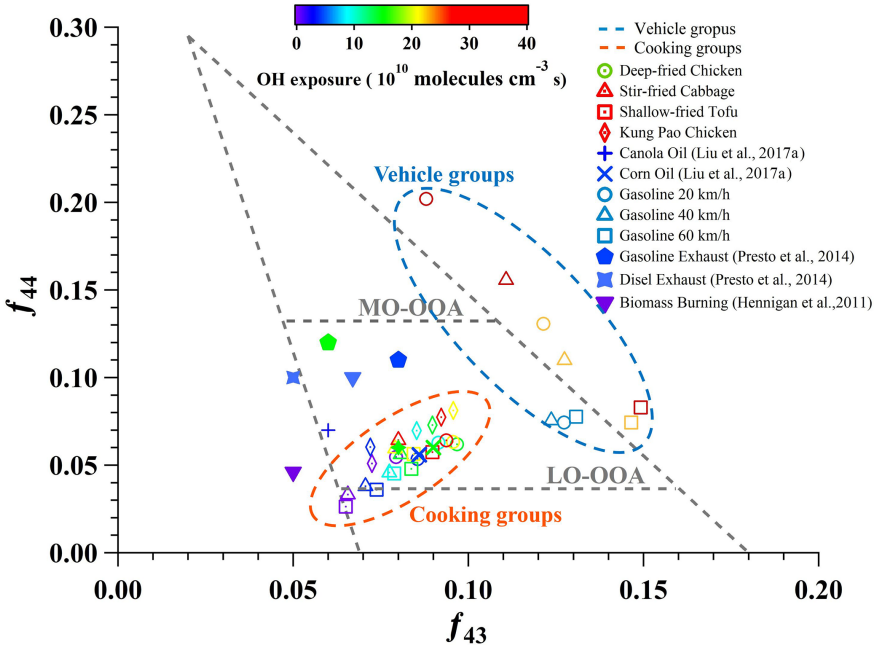

Figure 5. Fractions of entire organic signals at m/z 43 (f_{43}) vs. m/z 44 (f_{44}) from various sources as well as an Ng triangle plot. The f_{43} and f_{44} are determined by an HR-ToF-AMS. The average data at each gradient are shown in the figure.

insights into and references for those of ambient OAs observed in the atmosphere. Figure 7 plots the correlation coefficients between the aged laboratory OA and ambient PMF OA factors with growing photochemical ages (Li et al., 2020a). The field study was deployed at the Institute of Atmospheric Physics (IAP), Chinese Academy of Sciences (39°58′ N, 116°22′ E), in autumn and winter (autumn, 1 October–15 November 2018; winter, 5–31 January 2019) (Li et al., 2020a). The sample site is located on the south of Beitucheng West Road and west of Beijing–Chengde Expressway in Beijing, which is a typical urban site affected by local emissions (Li et al., 2020b). Table 6 exhibits correlations of mass spectra between laboratory results and ambient PMF factors, where the aged laboratory cooking OAs were divided into POAs and LO-OOAs, while the laboratory vehicle OAs were divided into LO-OOAs and MO-OOAs.

For the aged GDI OAs in Fig. 7, their average mass spectra retained some ambient HOA features (Pearson $r =$

Table 5. A summary of elemental ratios and dominant peaks among various SOAs.

Type	O/C	H/C	f_{28}	f_{29}	f_{41}	f_{43}	f_{44}	f_{55}	f_{57}	Dominant peaks (m/z in descending order)
GDI LO-OOA	0.46	1.80	0.066	0.076	0.051	0.133	0.077	0.043	0.029	43, 44, 29, 28, 41, 55
GDI MO-OOA	0.91	1.57	0.134	0.071	0.026	0.117	0.146	0.024	0.013	44, 28, 43, 29, 45, 27
Cooking LO-OOA	0.36	1.92	0.053	0.065	0.058	0.097	0.065	0.056	0.046	43, 44, 29, 41, 55, 28
Heated oil SOA (Liu et al., 2018)	0.38	1.53	0.070	0.087	0.067	0.078	0.067	0.053	0.023	29, 43, 28, 44, 41, 55
Meat charbroiling SOA (Kaltsonoudis et al., 2017)	0.24	1.83	0.039	0.061	0.077	0.075	0.052	0.074	0.035	41, 43, 55, 29, 27, 44
Gasoline SOA (Nordin et al., 2013)	0.40	1.38	0.122	0.032	0.031	0.094	0.129	0.019	0.008	44, 28, 39, 27, 29, 41
Diesel SOA (Chirico et al., 2010)	0.37	1.57	0.069	0.092	0.062	0.112	0.073	0.045	0.022	43, 29, 44, 28, 41, 27

Table 6. Pearson correlations between laboratory OA and ambient OA mass spectra.

Pearson correlation ($\alpha = 0.05$)	Ambient HOA	Ambient COA	Ambient LO-OOA	Ambient MO-OOA
Lab cooking POA	0.95	0.86	0.46	0.39
Lab cooking LO-OOA	0.90	0.81	0.76	0.68
Lab vehicle LO-OOA	0.80	0.71	0.81	0.73
Lab vehicle MO-OOA	0.54	0.44	0.98	0.94

0.80) under a low photochemical age of 0.6 d with moderate hydrocarbon-like ions such as m/z 41 and m/z 55, but they had already reached the same oxidation degree of ambient LO-OOAs (Pearson $r = 0.81$) with high O/C (0.46) and f_{43} (0.133). After aging in Go:PAM, the aged OAs might finally become a kind of ambient MO-OOA (Pearson $r = 0.97$) at 5.1 d of photochemical age. This evolution of GDI OAs (from HOAs to LO-OOAs to MO-OOAs) was similar to the result of a previous vehicle OA simulation (from HOAs to SV-OOAs to LV-OOAs) (Tkacik et al., 2014).

For the aged cooking OAs in Fig. 7, although their correlations with ambient LO-OOAs increased gradually from 0.56 to 0.73 along with the growing photochemical ages, their correlations with ambient COAs kept at a high level all the time (Pearson $r > 0.81$), implying a mixture of POAs and SOAs due to some hardly oxidized compounds emitted from the cooking process. Therefore, it is necessary to resolve aged cooking OA mass spectra comprehensively by PMF (Figs. S4–S11) and then compared their laboratory PMF results with ambient PMF factors. As Table 6 shows, the laboratory cooking POAs were similar to ambient COAs (Pearson $r = 0.86$) but less like LO-OOAs (Pearson $r = 0.46$) or MO-OOAs (Pearson $r = 0.39$). By contrast, the laboratory cooking LO-OOAs displayed many more ambient LO-OOA features (Pearson $r = 0.76$) and relatively fewer ambient COA characteristics than laboratory cooking POAs did. In short, these comparisons between laboratory and ambient results revealed that organics from these two urban-lifestyle sources might eventually form different SOA types in the real atmosphere.

4 Conclusions

In the present work, we define two urban-lifestyle SOAs in detail and investigate their mass growth potential, formation pathways, mass spectra, and chemical evolutions comprehensively. At about 2 d of equivalent photochemical age, the SOA/POA mass ratios of vehicle groups (107) were 44 times larger than those of cooking groups (2.38), and the O : C molar ratios of vehicle groups (0.66) were about 2 times as large as those of cooking groups (0.34). Besides, both vehicle and cooking groups may undergo an alcohol and/or peroxide pathway to form LO-OOAs, and the vehicle groups additionally undergo a carboxylic acid pathway to form a part of MO-OOAs. Furthermore, the characteristic mass spectra of these two urban-lifestyle SOAs could provide necessary references to estimate their mass fractions in ambient air, through a multilinear engine model (ME-2) (Canonaco et al., 2013; Qin et al., 2017). This application would reduce the large gaps of total atmospheric contributions and relevant environment effects for urban SOAs, although several uncertainties in SOA mass spectra remain due to missing complex mixture conditions in Go:PAM.

There are some uncertainties in our Go:PAM simulation. We focused more on the photochemical oxidation of SOAs under low RH levels, but aqueous-phase processing at high RH levels may also have impacts on SOA production. In the future, it will be better to strictly control the RH, high and low NO_x or SO_2, additional inorganic seeds, and so forth to thoroughly investigate how the aerosols age as a function of equivalent days of atmospheric oxidation. SVOCs and IVOCs may play important roles in forming SOAs but were

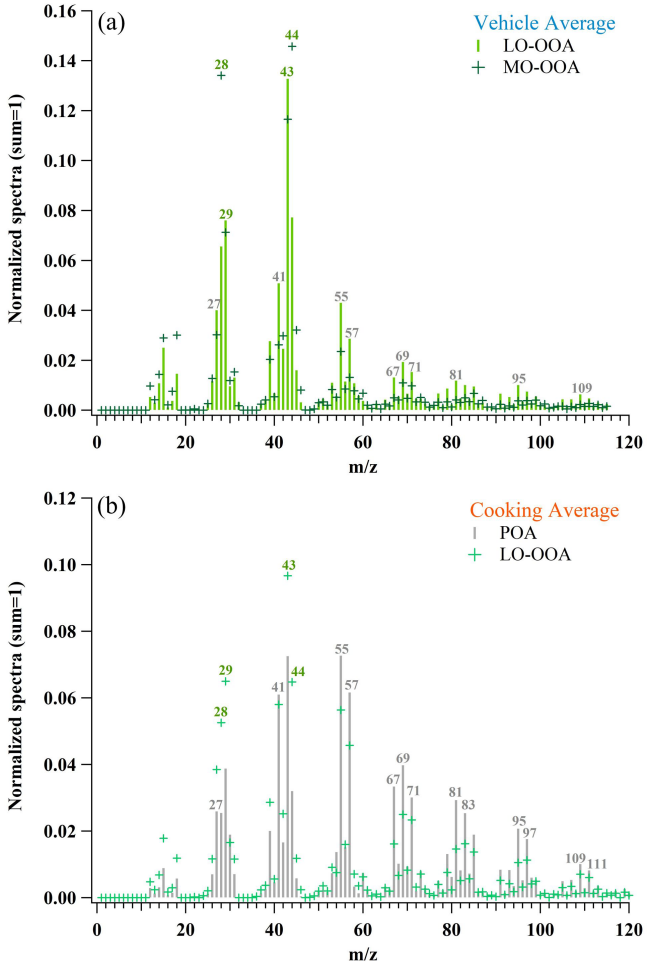

Figure 6. Average mass spectra of OAs from two urban-lifestyle sources. The numbered symbols represent the m/z values with relatively large fractions. The gray symbols represent the fragments that mainly come from hydrocarbon-like fragments, and the green symbols represent those that mainly come from oxygen-containing fragments. The mass spectra are determined by an HR-ToF-AMS. The average data are shown in the figure.

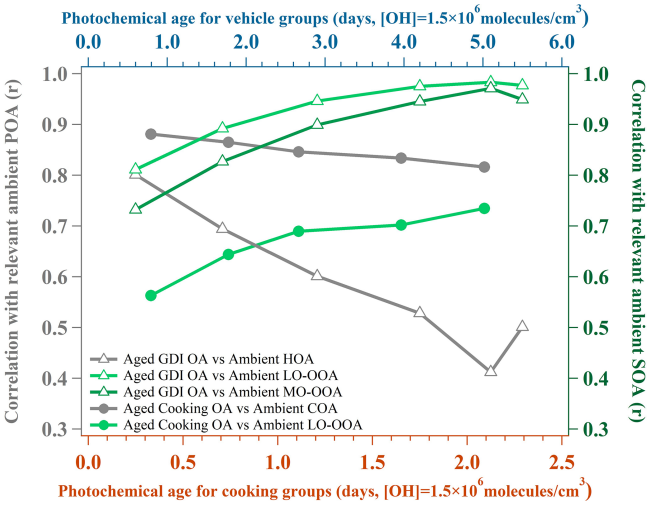

Figure 7. Correlation coefficients (Pearson r) between the aged laboratory OA and published ambient PMF OA factors with growing photochemical ages. Ambient PMF OA factors are the average results from two field studies in Beijing (measured at a typical urban site during autumn and winter; autumn, 1 October–15 November 2018; winter, 5–31 January 2019). The unit mass resolution mass spectra are determined by an HR-ToF-AMS.

partly lost in pipelines, and their sampling and quantification are extremely challenging, needing a more sophisticated experimental design. Moreover, the contribution of ozonolysis to SOA formation should be individually studied in further research. Furthermore, the relative strengths of the photochemical oxidation from gaseous precursors and the heterogeneous oxidation from POAs were not distinguished in depth in this work. Besides, it is recommended to add humidity to the carrier gas and turn on the lights during the OFR clean-out stage, in order to minimize the background concentration in Go:PAM.

Although strict policies have been implemented to reduce primary particulate matter (PM) in urban areas, secondary PM, especially for the abundant and complicated SOAs, is difficult to restrict (Wu et al., 2017; Li et al., 2018). According to our results, on the one hand, vehicle SOAs might be a mixture of both LO-OOAs and MO-OOAs with high secondary formation potential, so it would be better to not only filter out the exhaust PM with a gasoline particulate filter (GPF) but also reduce the gaseous precursors to restrict the secondary formation. On the other hand, cooking SOAs might comprise a kind of LO-OOA with relatively low secondary formation potential, so it could be enough to remove the gas and particle emissions at the same level. In the future, these two urban-lifestyle SOAs may present increasing contributions in urban areas especially in megacities with growing atmospheric oxidants (K. Li et al., 2019; Wang et al., 2017; Li et al., 2020a, b), but investigation of them and further management are far from sufficient, making it possible for this area to become a very meaningful research focus.

This work is an initial attempt to explore a series of studies on urban-lifestyle SOAs. In another companion publication currently in preparation (Song et al., 2021), gas- and particle-phase VOCs, SVOCs, and IVOCs from four typical Chinese domestic cuisines are quantified. It is found that 26 %–78 % of cooking SOAs could be explained from the oxidation of VOCs, SVOCs, and IVOCs. Moreover, oxygenated compounds, including acids, furans, amides, and esters, were the most abundant in the particle phase. In contrast, significant differences were found in the gas phase among four cuisines; for example, Kung Pao chicken and shallow-frying tofu showed a larger proportion of aromatics. Furthermore, we have attempted to apply the laboratory mass spectra from this work to the ambient air. The contributions of vehicle SOAs and cooking SOAs to OAs were estimated by an ME-

2 model in urban Beijing (Zhang et al., 2021). It was found that cooking SOAs (27 %–42 % of OAs) and vehicle SOAs (58 %–73 % of OAs) presented different diurnal patterns, implying their different formation pathways. Similar features of urban-lifestyle SOAs were found between laboratory and field results.

Data availability. The data provided in this paper can be obtained from the author upon request (minhu@pku.edu.cn).

Supplement. The supplement related to this article is available online at: https://doi.org/10.5194/acp-21-15221-2021-supplement.

Author contributions. ZiZ contributed in terms of investigation, data curation, methodology, formal analysis, writing of the original draft, and writing – review and editing. WenfZ contributed in terms of investigation, data curation, methodology, formal analysis, and writing – review and editing. MH contributed in terms of project administration, supervision, funding acquisition, and writing – review and editing. KL contributed in terms of investigation, data curation, and formal analysis. HW, RoT, RS, YY, RuT, KS, YL, WenbZ, and ZhZ contributed in terms of investigation and data curation. HX, SS, SL, YC, JL, and YW contributed in terms of data curation. SG contributed in terms of project administration, funding acquisition, and writing – review and editing.

Competing interests. The authors declare that they have no known competing financial interests or personal relationships that could have influenced the work reported in this paper.

Disclaimer. Publisher's note: Copernicus Publications remains neutral with regard to jurisdictional claims in published maps and institutional affiliations.

Acknowledgements. Thanks to all the researchers from PKU who had directly participated in the main laboratory simulation. Thanks to all the researchers from THU and CAS who provided the necessary experiment sites, instruments, and data support.

Financial support. The research has been supported by the National Key R&D Program of China (2016YFC0202000), National Natural Science Foundation of China (51636003, 91844301, 41977179, and 21677002), Beijing Municipal Science and Technology Commission (Z201100008220011), Open Research Fund of State Key Laboratory of Multiphase Complex Systems (MPCS-2019-D-09), and China Postdoctoral Science Foundation (2020M680242).

Review statement. This paper was edited by James Allan and reviewed by three anonymous referees.

References

Alanen, J., Simonen, P., Saarikoski, S., Timonen, H., Kangasniemi, O., Saukko, E., Hillamo, R., Lehtoranta, K., Murtonen, T., Vesala, H., Keskinen, J., and Rönkkö, T.: Comparison of primary and secondary particle formation from natural gas engine exhaust and of their volatility characteristics, Atmos. Chem. Phys., 17, 8739–8755, https://doi.org/10.5194/acp-17-8739-2017, 2017.

Allan, J. D., Williams, P. I., Morgan, W. T., Martin, C. L., Flynn, M. J., Lee, J., Nemitz, E., Phillips, G. J., Gallagher, M. W., and Coe, H.: Contributions from transport, solid fuel burning and cooking to primary organic aerosols in two UK cities, Atmos. Chem. Phys., 10, 647–668, https://doi.org/10.5194/acp-10-647-2010, 2010.

An, Z., Huang, R. J., Zhang, R., Tie, X., Li, G., Cao, J., Zhou, W., Shi, Z., Han, Y., Gu, Z., and Ji, Y.: Severe haze in northern China: A synergy of anthropogenic emissions and atmospheric processes, P. Natl. Acad. Sci. USA, 116, 8657-8666, https://doi.org/10.1073/pnas.1900125116, 2019.

Canonaco, F., Crippa, M., Slowik, J. G., Baltensperger, U., and Prévôt, A. S. H.: SoFi, an IGOR-based interface for the efficient use of the generalized multilinear engine (ME-2) for the source apportionment: ME-2 application to aerosol mass spectrometer data, Atmos. Meas. Tech., 6, 3649–3661, https://doi.org/10.5194/amt-6-3649-2013, 2013.

Chan, C. K., and Yao, X.: Air pollution in mega cities in China, Atmos. Environ., 42, 1–42, https://doi.org/10.1016/j.atmosenv.2007.09.003, 2008.

Chirico, R., DeCarlo, P. F., Heringa, M. F., Tritscher, T., Richter, R., Prévôt, A. S. H., Dommen, J., Weingartner, E., Wehrle, G., Gysel, M., Laborde, M., and Baltensperger, U.: Impact of aftertreatment devices on primary emissions and secondary organic aerosol formation potential from in-use diesel vehicles: results from smog chamber experiments, Atmos. Chem. Phys., 10, 11545–11563, https://doi.org/10.5194/acp-10-11545-2010, 2010.

Crippa, M., DeCarlo, P. F., Slowik, J. G., Mohr, C., Heringa, M. F., Chirico, R., Poulain, L., Freutel, F., Sciare, J., Cozic, J., Di Marco, C. F., Elsasser, M., Nicolas, J. B., Marchand, N., Abidi, E., Wiedensohler, A., Drewnick, F., Schneider, J., Borrmann, S., Nemitz, E., Zimmermann, R., Jaffrezo, J.-L., Prévôt, A. S. H., and Baltensperger, U.: Wintertime aerosol chemical composition and source apportionment of the organic fraction in the metropolitan area of Paris, Atmos. Chem. Phys., 13, 961–981, https://doi.org/10.5194/acp-13-961-2013, 2013.

DeCarlo, P. F., Kimmel, J. R., Trimborn, A., Northway, M. J., Jayne, J. T., Aiken, A. C., Gonin, M., Fuhrer, K., Horvath, T., Docherty, K. S., Worsnop, D. R., and Jimenez, J. L.: Field-deployable, high-resolution, time-of-flight aerosol mass spectrometer, Anal. Chem., 78, 8281–8289, https://doi.org/10.1021/ac061249n, 2006.

de Gouw, J. A., Brock, C. A., Atlas, E. L., Bates, T. S., Fehsenfeld, F. C., Goldan, P. D., Holloway, J. S., Kuster, W. C., Lerner, B. M., Matthew, B. M., Middlebrook, A. M., Onasch, T. B., Peltier, R. E., Quinn, P. K., Senff, C. J., Stohl, A., Sullivan, A. P., Trainer, M., Warneke, C., Weber, R. J., and Williams, E. J.: Sources of particulate matter in the northeastern United States in summer: 1. Direct emissions and secondary formation of organic matter in urban plumes, J. Geophys. Res., 113, D08301, https://doi.org/10.1029/2007jd009243, 2008.

Deming, B. L., Pagonis, D., Liu, X., Day, D. A., Talukdar, R., Krechmer, J. E., de Gouw, J. A., Jimenez, J. L., and Ziemann, P. J.: Measurements of delays of gas-phase compounds in a wide variety of tubing materials due to gas–wall interactions, Atmos. Meas. Tech., 12, 3453–3461, https://doi.org/10.5194/amt-12-3453-2019, 2019.

Deng, W., Fang, Z., Wang, Z., Zhu, M., Zhang, Y., Tang, M., Song, W., Lowther, S., Huang, Z., Jones, K., Peng, P., and Wang, X.: Primary emissions and secondary organic aerosol formation from in-use diesel vehicle exhaust: Comparison between idling and cruise mode, Sci. Total Environ., 699, 134357, https://doi.org/10.1016/j.scitotenv.2019.134357, 2020.

Donahue, N. M., Robinson, A. L., and Pandis, S. N.: Atmospheric organic particulate matter: From smoke to secondary organic aerosol, Atmos. Environ., 43, 94–106, https://doi.org/10.1016/j.atmosenv.2008.09.055, 2009.

Drewnick, F., Hings, S. S., DeCarlo, P., Jayne, J. T., Gonin, M., Fuhrer, K., Weimer, S., Jimenez, J. L., Demerjian, K. L., Borrmann, S., and Worsnop, D. R.: A New Time-of-Flight Aerosol Mass Spectrometer (TOF-AMS) – Instrument Description and First Field Deployment, Aerosol Sci. Tech., 39, 637–658, https://doi.org/10.1080/02786820500182040, 2005.

Du, Z., Hu, M., Peng, J., Zhang, W., Zheng, J., Gu, F., Qin, Y., Yang, Y., Li, M., Wu, Y., Shao, M., and Shuai, S.: Comparison of primary aerosol emission and secondary aerosol formation from gasoline direct injection and port fuel injection vehicles, Atmos. Chem. Phys., 18, 9011–9023, https://doi.org/10.5194/acp-18-9011-2018, 2018.

Esmaeilirad, S. and Hosseini, V.: Modeling the formation of traditional and non-traditional secondary organic aerosols from in-use, on-road gasoline and diesel vehicles exhaust, J. Aerosol Sci., 124, 68–82, https://doi.org/10.1016/j.jaerosci.2018.07.003, 2018.

Ge, X., Setyan, A., Sun, Y., and Zhang, Q.: Primary and secondary organic aerosols in Fresno, California during wintertime: Results from high resolution aerosol mass spectrometry, J. Geophys. Res.-Atmos., 117, D19301, https://doi.org/10.1029/2012jd018026, 2012.

Gordon, T. D., Tkacik, D. S., Presto, A. A., Zhang, M., Jathar, S. H., Nguyen, N. T., Massetti, J., Truong, T., Cicero-Fernandez, P., Maddox, C., Rieger, P., Chattopadhyay, S., Maldonado, H., Maricq, M. M., and Robinson, A. L.: Primary gas- and particle-phase emissions and secondary organic aerosol production from gasoline and diesel off-road engines, Environ. Sci. Technol., 47, 14137–14146, https://doi.org/10.1021/es403556e, 2013.

Guo, S., Hu, M., Guo, Q., Zhang, X., Zheng, M., Zheng, J., Chang, C. C., Schauer, J. J., and Zhang, R.: Primary sources and secondary formation of organic aerosols in Beijing, China, Environ. Sci. Technol., 46, 9846–9853, https://doi.org/10.1021/es2042564, 2012.

Guo, S., Hu, M., Guo, Q., Zhang, X., Schauer, J. J., and Zhang, R.: Quantitative evaluation of emission controls on primary and secondary organic aerosol sources during Beijing 2008 Olympics, Atmos. Chem. Phys., 13, 8303–8314, https://doi.org/10.5194/acp-13-8303-2013, 2013.

Guo, S., Hu, M., Zamora, M. L., Peng, J. F., Shang, D. J., Zheng, J., Du, Z. F., Wu, Z., Shao, M., Zeng, L. M., Molina, M. J., and Zhang, R. Y.: Elucidating severe urban haze formation in China, P. Natl. Acad. Sci. USA, 111, 17373–17378, https://doi.org/10.1073/pnas.1419604111, 2014.

Guo, S., Hu, M., Peng, J. F., Wu, Z. J., Zamora, M. L., Shang, D. J., Du, Z. F., Zheng, J., Fang, X., Tang, R. Z., Wu, Y. S., Zeng, L. M., Shuai, S. J., Zhang, W. B., Wang, Y., Ji, Y. M., Li, Y. X., Zhang, A. L., Wang, W. G., Zhang, F., Zhao, J. Y., Gong, X. L., Wang, C. Y., Molina, M. J., and Zhang, R. Y.: Remarkable nucleation and growth of ultrafine particles from vehicular exhaust, P. Natl. Acad. Sci. USA, 117, 3427–3432, https://doi.org/10.1073/pnas.1916366117, 2020.

Hallquist, M., Munthe, J., Hu, M., Wang, T., Chan, C. K., Gao, J., Boman, J., Guo, S., Hallquist, A. M., Mellqvist, J., Moldanova, J., Pathak, R. K., Pettersson, J. B. C., Pleijel, H., Simpson, D., and Thynell, M.: Photochemical smog in China: scientific challenges and implications for air-quality policies, Natl. Sci. Rev., 3, 401–403, https://doi.org/10.1093/nsr/nww080, 2016.

Hayes, P. L., Carlton, A. G., Baker, K. R., Ahmadov, R., Washenfelder, R. A., Alvarez, S., Rappenglück, B., Gilman, J. B., Kuster, W. C., de Gouw, J. A., Zotter, P., Prévôt, A. S. H., Szidat, S., Kleindienst, T. E., Offenberg, J. H., Ma, P. K., and Jimenez, J. L.: Modeling the formation and aging of secondary organic aerosols in Los Angeles during CalNex 2010, Atmos. Chem. Phys., 15, 5773–5801, https://doi.org/10.5194/acp-15-5773-2015, 2015.

Heald, C. L., Kroll, J. H., Jimenez, J. L., Docherty, K. S., DeCarlo, P. F., Aiken, A. C., Chen, Q., Martin, S. T., Farmer, D. K., and Artaxo, P.: A simplified description of the evolution of organic aerosol composition in the atmosphere, Geophys. Res. Lett., 37, L08803, https://doi.org/10.1029/2010gl042737, 2010.

Hennigan, C. J., Miracolo, M. A., Engelhart, G. J., May, A. A., Presto, A. A., Lee, T., Sullivan, A. P., McMeeking, G. R., Coe, H., Wold, C. E., Hao, W.-M., Gilman, J. B., Kuster, W. C., de Gouw, J., Schichtel, B. A., Collett Jr., J. L., Kreidenweis, S. M., and Robinson, A. L.: Chemical and physical transformations of organic aerosol from the photo-oxidation of open biomass burning emissions in an environmental chamber, Atmos. Chem. Phys., 11, 7669–7686, https://doi.org/10.5194/acp-11-7669-2011, 2011.

Hu, M., Guo, S., Peng, J. F., and Wu, Z. J.: Insight into characteristics and sources of $PM_{2.5}$ in the Beijing-Tianjin-Hebei region, China, Natl. Sci. Rev., 2, 257–258, https://doi.org/10.1093/nsr/nwv003, 2015.

Hu, W., Hu, M., Hu, W.-W., Zheng, J., Chen, C., Wu, Y., and Guo, S.: Seasonal variations in high time-resolved chemical compositions, sources, and evolution of atmospheric submicron aerosols in the megacity Beijing, Atmos. Chem. Phys., 17, 9979–10000, https://doi.org/10.5194/acp-17-9979-2017, 2017.

Jayne, J. T., Leard, D. C., Zhang, X., Davidovits, P., Smith, K. A., Kolb, C. E., and Worsnop, D. R.: Development of an Aerosol Mass Spectrometer for Size and Composition Analysis of Submicron Particles, Aerosol Sci. Technol., 33, 49–70, https://doi.org/10.1080/027868200410840, 2000.

Jimenez, J. L., Canagaratna, M. R., Donahue, N. M., Prevot, A. S., Zhang, Q., Kroll, J. H., DeCarlo, P. F., Allan, J. D., Coe, H., Ng, N. L., Aiken, A. C., Docherty, K. S., Ulbrich, I. M., Grieshop, A. P., Robinson, A. L., Duplissy, J., Smith, J. D., Wilson, K. R., Lanz, V. A., Hueglin, C., Sun, Y. L., Tian, J., Laaksonen, A., Raatikainen, T., Rautiainen, J., Vaattovaara, P., Ehn, M., Kulmala, M., Tomlinson, J. M., Collins, D. R., Cubison, M. J., Dunlea, E. J., Huffman, J. A., Onasch, T. B., Al-

farra, M. R., Williams, P. I., Bower, K., Kondo, Y., Schneider, J., Drewnick, F., Borrmann, S., Weimer, S., Demerjian, K., Salcedo, D., Cottrell, L., Griffin, R., Takami, A., Miyoshi, T., Hatakeyama, S., Shimono, A., Sun, J. Y., Zhang, Y. M., Dzepina, K., Kimmel, J. R., Sueper, D., Jayne, J. T., Herndon, S. C., Trimborn, A. M., Williams, L. R., Wood, E. C., Middlebrook, A. M., Kolb, C. E., Baltensperger, U., and Worsnop, D. R.: Evolution of organic aerosols in the atmosphere, Science, 326, 1525–1529, https://doi.org/10.1126/science.1180353, 2009.

Kaltsonoudis, C., Kostenidou, E., Louvaris, E., Psichoudaki, M., Tsiligiannis, E., Florou, K., Liangou, A., and Pandis, S. N.: Characterization of fresh and aged organic aerosol emissions from meat charbroiling, Atmos. Chem. Phys., 17, 7143–7155, https://doi.org/10.5194/acp-17-7143-2017, 2017.

Katragadda, H. R., Fullana, A., Sidhu, S., and Carbonell-Barrachina, Á. A.: Emissions of volatile aldehydes from heated cooking oils, Food Chem., 120, 59–65, https://doi.org/10.1016/j.foodchem.2009.09.070, 2010.

Kim, C., Gao, Y. T., Xiang, Y. B., Barone-Adesi, F., Zhang, Y., Hosgood, H. D., Ma, S., Shu, X. O., Ji, B. T., Chow, W. H., Seow, W. J., Bassig, B., Cai, Q., Zheng, W., Rothman, N., and Lan, Q.: Home kitchen ventilation, cooking fuels, and lung cancer risk in a prospective cohort of never smoking women in Shanghai, China, Int. J. Cancer, 136, 632–638, https://doi.org/10.1002/ijc.29020, 2015.

Klein, F., Platt, S. M., Farren, N. J., Detournay, A., Bruns, E. A., Bozzetti, C., Daellenbach, K. R., Kilic, D., Kumar, N. K., Pieber, S. M., Slowik, J. G., Temime-Roussel, B., Marchand, N., Hamilton, J. F., Baltensperger, U., Prevot, A. S., and El Haddad, I.: Characterization of Gas-Phase Organics Using Proton Transfer Reaction Time-of-Flight Mass Spectrometry: Cooking Emissions, Environ. Sci. Technol., 50, 1243–1250, https://doi.org/10.1021/acs.est.5b04618, 2016.

Kleinman, L. I., Springston, S. R., Daum, P. H., Lee, Y.-N., Nunnermacker, L. J., Senum, G. I., Wang, J., Weinstein-Lloyd, J., Alexander, M. L., Hubbe, J., Ortega, J., Canagaratna, M. R., and Jayne, J.: The time evolution of aerosol composition over the Mexico City plateau, Atmos. Chem. Phys., 8, 1559–1575, https://doi.org/10.5194/acp-8-1559-2008, 2008.

Lambe, A. T., Ahern, A. T., Williams, L. R., Slowik, J. G., Wong, J. P. S., Abbatt, J. P. D., Brune, W. H., Ng, N. L., Wright, J. P., Croasdale, D. R., Worsnop, D. R., Davidovits, P., and Onasch, T. B.: Characterization of aerosol photooxidation flow reactors: heterogeneous oxidation, secondary organic aerosol formation and cloud condensation nuclei activity measurements, Atmos. Meas. Tech., 4, 445–461, https://doi.org/10.5194/amt-4-445-2011, 2011.

Lee, B. P., Li, Y. J., Yu, J. Z., Louie, P. K. K., and Chan, C. K.: Characteristics of submicron particulate matter at the urban roadside in downtown Hong Kong-Overview of 4 months of continuous high-resolution aerosol mass spectrometer measurements, J. Geophys. Res.-Atmos., 120, 7040–7058, https://doi.org/10.1002/2015jd023311, 2015.

Li, J., Li, X.-B., Li, B., and Peng, Z.-R.: The Effect of Nonlocal Vehicle Restriction Policy on Air Quality in Shanghai, Atmosphere, 9, 299, https://doi.org/10.3390/atmos9080299, 2018.

Li, J., Liu, Q., Li, Y., Liu, T., Huang, D., Zheng, J., Zhu, W., Hu, M., Wu, Y., Lou, S., Hallquist, Å. M., Hallquist, M., Chan, C. K., Canonaco, F., Prévôt, A. S. H., Fung, J. C. H., Lau, A. K. H., and Yu, J. Z.: Characterization of Aerosol Aging Potentials at Suburban Sites in Northern and Southern China Utilizing a Potential Aerosol Mass (Go:PAM) Reactor and an Aerosol Mass Spectrometer, J. Geophys. Res.-Atmos., 124, 5629–5649, https://doi.org/10.1029/2018jd029904, 2019.

Li, J., Gao, W., Cao, L., Xiao, Y., Zhang, Y., Zhao, S., Liu, Z., Liu, Z., Tang, G., Ji, D., bo, H., Song, T., He, L., Hu, M., and Wang, Y.: Significant changes in autumn and winter aerosol composition and sources in Beijing from 2012 to 2018: effects of clean air actions, Environ. Pollut., 268, 115855, https://doi.org/10.1016/j.envpol.2020.115855, 2020a.

Li, J., Liu, Z., Gao, W., Tang, G., Hu, B., Ma, Z., and Wang, Y.: Insight into the formation and evolution of secondary organic aerosol in the megacity of Beijing, China, Atmos. Environ., 220, 117070, https://doi.org/10.1016/j.atmosenv.2019.117070, 2020b.

Li, K., Jacob, D. J., Liao, H., Shen, L., Zhang, Q., and Bates, K. H.: Anthropogenic drivers of 2013–2017 trends in summer surface ozone in China, P. Natl. Acad. Sci. USA, 116, 422–427, https://doi.org/10.1073/pnas.1812168116, 2019.

Liao, K., Chen, Q., Liu, Y., Li, Y. J., Lambe, A. T., Zhu, T., Huang, R. J., Zheng, Y., Cheng, X., Miao, R., Huang, G., Khuzestani, R. B., and Jia, T.: Secondary Organic Aerosol Formation of Fleet Vehicle Emissions in China: Potential Seasonality of Spatial Distributions, Environ. Sci. Technol., 55, 7276–7286, https://doi.org/10.1021/acs.est.0c08591, 2021.

Lim, C. Y., Hagan, D. H., Coggon, M. M., Koss, A. R., Sekimoto, K., de Gouw, J., Warneke, C., Cappa, C. D., and Kroll, J. H.: Secondary organic aerosol formation from the laboratory oxidation of biomass burning emissions, Atmos. Chem. Phys., 19, 12797–12809, https://doi.org/10.5194/acp-19-12797-2019, 2019.

Liu, T., Li, Z., Chan, M., and Chan, C. K.: Formation of secondary organic aerosols from gas-phase emissions of heated cooking oils, Atmos. Chem. Phys., 17, 7333–7344, https://doi.org/10.5194/acp-17-7333-2017, 2017a.

Liu, T., Liu, Q., Li, Z., Huo, L., Chan, M., Li, X., Zhou, Z., and Chan, C. K.: Emission of volatile organic compounds and production of secondary organic aerosol from stir-frying spices, Sci. Total Environ., 599–600, 1614–1621, https://doi.org/10.1016/j.scitotenv.2017.05.147, 2017b.

Liu, T., Wang, Z., Huang, D. D., Wang, X., and Chan, C. K.: Significant Production of Secondary Organic Aerosol from Emissions of Heated Cooking Oils, Environ. Sci. Tech. Let., 5, 32–37, https://doi.org/10.1021/acs.estlett.7b00530, 2017c.

Liu, T., Wang, Z., Wang, X., and Chan, C. K.: Primary and secondary organic aerosol from heated cooking oil emissions, Atmos. Chem. Phys., 18, 11363–11374, https://doi.org/10.5194/acp-18-11363-2018, 2018.

Liu, T., Zhou, L., Liu, Q., Lee, B. P., Yao, D., Lu, H., Lyu, X., Guo, H., and Chan, C. K.: Secondary Organic Aerosol Formation from Urban Roadside Air in Hong Kong, Environ. Sci. Technol., 53, 3001–3009, https://doi.org/10.1021/acs.est.8b06587, 2019.

Mao, J., Ren, X., Brune, W. H., Olson, J. R., Crawford, J. H., Fried, A., Huey, L. G., Cohen, R. C., Heikes, B., Singh, H. B., Blake, D. R., Sachse, G. W., Diskin, G. S., Hall, S. R., and Shetter, R. E.: Airborne measurement of OH reactivity during INTEX-B, Atmos. Chem. Phys., 9, 163–173, https://doi.org/10.5194/acp-9-163-2009, 2009.

Masuda, M., Wang, Q., Tokumura, M., Miyake, Y., and Amagai, T.: Risk assessment of polycyclic aromatic hydrocarbons and their chlorinated derivatives produced during cooking and released in exhaust gas, Ecotox. Environ. Safe., 197, 110592, https://doi.org/10.1016/j.ecoenv.2020.110592, 2020.

Matsui, H., Koike, M., Takegawa, N., Kondo, Y., Griffin, R. J., Miyazaki, Y., Yokouchi, Y., and Ohara, T.: Secondary organic aerosol formation in urban air: Temporal variations and possible contributions from unidentified hydrocarbons, J. Geophys. Res., 114, D04201, https://doi.org/10.1029/2008jd010164, 2009.

Mohr, C., DeCarlo, P. F., Heringa, M. F., Chirico, R., Slowik, J. G., Richter, R., Reche, C., Alastuey, A., Querol, X., Seco, R., Peñuelas, J., Jiménez, J. L., Crippa, M., Zimmermann, R., Baltensperger, U., and Prévôt, A. S. H.: Identification and quantification of organic aerosol from cooking and other sources in Barcelona using aerosol mass spectrometer data, Atmos. Chem. Phys., 12, 1649–1665, https://doi.org/10.5194/acp-12-1649-2012, 2012.

Nash, D. G., Baer, T., and Johnston, M. V.: Aerosol mass spectrometry: An introductory review, Int. J. Mass Spectrom., 258, 2–12, https://doi.org/10.1016/j.ijms.2006.09.017, 2006.

Ng, N. L., Canagaratna, M. R., Zhang, Q., Jimenez, J. L., Tian, J., Ulbrich, I. M., Kroll, J. H., Docherty, K. S., Chhabra, P. S., Bahreini, R., Murphy, S. M., Seinfeld, J. H., Hildebrandt, L., Donahue, N. M., DeCarlo, P. F., Lanz, V. A., Prévôt, A. S. H., Dinar, E., Rudich, Y., and Worsnop, D. R.: Organic aerosol components observed in Northern Hemispheric datasets from Aerosol Mass Spectrometry, Atmos. Chem. Phys., 10, 4625–4641, https://doi.org/10.5194/acp-10-4625-2010, 2010.

Ng, N. L., Canagaratna, M. R., Jimenez, J. L., Zhang, Q., Ulbrich, I. M., and Worsnop, D. R.: Real-Time Methods for Estimating Organic Component Mass Concentrations from Aerosol Mass Spectrometer Data, Environ. Sci. Technol., 45, 910-916, https://doi.org/10.1021/es102951k, 2011.

Nordin, E. Z., Eriksson, A. C., Roldin, P., Nilsson, P. T., Carlsson, J. E., Kajos, M. K., Hellén, H., Wittbom, C., Rissler, J., Löndahl, J., Swietlicki, E., Svenningsson, B., Bohgard, M., Kulmala, M., Hallquist, M., and Pagels, J. H.: Secondary organic aerosol formation from idling gasoline passenger vehicle emissions investigated in a smog chamber, Atmos. Chem. Phys., 13, 6101–6116, https://doi.org/10.5194/acp-13-6101-2013, 2013.

Peng, Z., Day, D. A., Ortega, A. M., Palm, B. B., Hu, W., Stark, H., Li, R., Tsigaridis, K., Brune, W. H., and Jimenez, J. L.: Non-OH chemistry in oxidation flow reactors for the study of atmospheric chemistry systematically examined by modeling, Atmos. Chem. Phys., 16, 4283–4305, https://doi.org/10.5194/acp-16-4283-2016, 2016.

Presto, A. A., Gordon, T. D., and Robinson, A. L.: Primary to secondary organic aerosol: evolution of organic emissions from mobile combustion sources, Atmos. Chem. Phys., 14, 5015–5036, https://doi.org/10.5194/acp-14-5015-2014, 2014.

Qin, Y. M., Tan, H. B., Li, Y. J., Schurman, M. I., Li, F., Canonaco, F., Prévôt, A. S. H., and Chan, C. K.: Impacts of traffic emissions on atmospheric particulate nitrate and organics at a downwind site on the periphery of Guangzhou, China, Atmos. Chem. Phys., 17, 10245–10258, https://doi.org/10.5194/acp-17-10245-2017, 2017.

Rogge, W. F., Hildemann, L. M., Mazurek, M. A., Cass, G. R., and Simonelt, B. R. T.: Sources of fine organic aerosol .1. charbroilers and meat cooking operations, Environ. Sci. Technol., 25, 1112–1125, https://doi.org/10.1021/es00018a015, 1991.

Rogge, W. F., Hildemann, L. M., Mazurek, M. A., Cass, G. R., and Simoneit, B. R. T.: Sources of fine organic aerosol .2. noncatalyst and catalyst-equipped automobiles and heavy-duty diesel trucks, Environ. Sci. Technol., 27, 636–651, https://doi.org/10.1021/es00041a007, 1993.

Seow, A., Poh, W. T., Teh, M., Eng, P., Wang, Y. T., Tan, W. C., Yu, M. C., and Lee, H. P.: Fumes from meat cooking and lung cancer risk in Chinese women, Cancer Epidemiol. Biomarkers Prev., 9, 1215–1221, 2000.

Song, K., Guo, S., et al.: Cooking emitted S/IVOCs are a large pool of SOA formation precursors, in preparation, 2021.

Suarez-Bertoa, R., Zardini, A. A., Platt, S. M., Hellebust, S., Pieber, S. M., El Haddad, I., Temime-Roussel, B., Baltensperger, U., Marchand, N., Prévôt, A. S. H., and Astorga, C.: Primary emissions and secondary organic aerosol formation from the exhaust of a flex-fuel (ethanol) vehicle, Atmospheric Environment, 117, 200-211, https://doi.org/10.1016/j.atmosenv.2015.07.006, 2015.

Sun, Y.-L., Zhang, Q., Schwab, J. J., Demerjian, K. L., Chen, W.-N., Bae, M.-S., Hung, H.-M., Hogrefe, O., Frank, B., Rattigan, O. V., and Lin, Y.-C.: Characterization of the sources and processes of organic and inorganic aerosols in New York city with a high-resolution time-of-flight aerosol mass apectrometer, Atmos. Chem. Phys., 11, 1581–1602, https://doi.org/10.5194/acp-11-1581-2011, 2011.

Sun, Y. L., Zhang, Q., Schwab, J. J., Chen, W.-N., Bae, M.-S., Hung, H.-M., Lin, Y.-C., Ng, N. L., Jayne, J., Massoli, P., Williams, L. R., and Demerjian, K. L.: Characterization of near-highway submicron aerosols in New York City with a high-resolution aerosol mass spectrometer, Atmos. Chem. Phys., 12, 2215–2227, https://doi.org/10.5194/acp-12-2215-2012, 2012.

Tang, R. Z., Wang, H., Liu, Y., and Guo, S.: Constituents of Atmospheric Semi-Volatile and Intermediate Volatility Organic Compounds and Their Contribution to Organic Aerosol, Prog. Chem., 31, 1800-190, https://doi.org/10.7536/pc180431, 2019.

Timonen, H., Karjalainen, P., Saukko, E., Saarikoski, S., Aakko-Saksa, P., Simonen, P., Murtonen, T., Dal Maso, M., Kuuluvainen, H., Bloss, M., Ahlberg, E., Svenningsson, B., Pagels, J., Brune, W. H., Keskinen, J., Worsnop, D. R., Hillamo, R., and Rönkkö, T.: Influence of fuel ethanol content on primary emissions and secondary aerosol formation potential for a modern flex-fuel gasoline vehicle, Atmos. Chem. Phys., 17, 5311–5329, https://doi.org/10.5194/acp-17-5311-2017, 2017.

Tkacik, D. S., Lambe, A. T., Jathar, S., Li, X., Presto, A. A., Zhao, Y., Blake, D., Meinardi, S., Jayne, J. T., Croteau, P. L., and Robinson, A. L.: Secondary organic aerosol formation from in-use motor vehicle emissions using a potential aerosol mass reactor, Environ. Sci. Technol., 48, 11235–11242, https://doi.org/10.1021/es502239v, 2014.

Ulbrich, I. M., Canagaratna, M. R., Zhang, Q., Worsnop, D. R., and Jimenez, J. L.: Interpretation of organic components from Positive Matrix Factorization of aerosol mass spectrometric data, Atmos. Chem. Phys., 9, 2891–2918, https://doi.org/10.5194/acp-9-2891-2009, 2009.

Vesna, O., Sax, M., Kalberer, M., Gaschen, A., and Ammann, M.: Product study of oleic acid ozonolysis as function of humidity, Atmos. Environ., 43, 3662–3669, https://doi.org/10.1016/j.atmosenv.2009.04.047, 2009.

Volkamer, R., Jimenez, J. L., San Martini, F., Dzepina, K., Zhang, Q., Salcedo, D., Molina, L. T., Worsnop, D. R., and Molina, M. J.: Secondary organic aerosol formation from anthropogenic air pollution: Rapid and higher than expected, Geophys. Res. Lett., 33, L17811, https://doi.org/10.1029/2006gl026899, 2006.

Wang, T., Xue, L., Brimblecombe, P., Lam, Y. F., Li, L., and Zhang, L.: Ozone pollution in China: A review of concentrations, meteorological influences, chemical precursors, and effects, Sci. Total Environ., 575, 1582–1596, https://doi.org/10.1016/j.scitotenv.2016.10.081, 2017.

Watne, A. K., Psichoudaki, M., Ljungstrom, E., Le Breton, M., Hallquist, M., Jerksjo, M., Fallgren, H., Jutterstrom, S., and Hallquist, A. M.: Fresh and Oxidized Emissions from In-Use Transit Buses Running on Diesel, Biodiesel, and CNG, Environ. Sci. Technol., 52, 7720–7728, https://doi.org/10.1021/acs.est.8b01394, 2018.

Wei, W., Cheng, S., Li, G., Wang, G., and Wang, H.: Characteristics of ozone and ozone precursors (VOCs and NOx) around a petroleum refinery in Beijing, China, J. Environ. Sci., 26, 332–342, https://doi.org/10.1016/s1001-0742(13)60412-x, 2014.

Wiedensohler, A., Birmili, W., Nowak, A., Sonntag, A., Weinhold, K., Merkel, M., Wehner, B., Tuch, T., Pfeifer, S., Fiebig, M., Fjäraa, A. M., Asmi, E., Sellegri, K., Depuy, R., Venzac, H., Villani, P., Laj, P., Aalto, P., Ogren, J. A., Swietlicki, E., Williams, P., Roldin, P., Quincey, P., Hüglin, C., Fierz-Schmidhauser, R., Gysel, M., Weingartner, E., Riccobono, F., Santos, S., Grüning, C., Faloon, K., Beddows, D., Harrison, R., Monahan, C., Jennings, S. G., O'Dowd, C. D., Marinoni, A., Horn, H.-G., Keck, L., Jiang, J., Scheckman, J., McMurry, P. H., Deng, Z., Zhao, C. S., Moerman, M., Henzing, B., de Leeuw, G., Löschau, G., and Bastian, S.: Mobility particle size spectrometers: harmonization of technical standards and data structure to facilitate high quality long-term observations of atmospheric particle number size distributions, Atmos. Meas. Tech., 5, 657–685, https://doi.org/10.5194/amt-5-657-2012, 2012.

Wu, Y., Zhang, S., Hao, J., Liu, H., Wu, X., Hu, J., Walsh, M. P., Wallington, T. J., Zhang, K. M., and Stevanovic, S.: On-road vehicle emissions and their control in China: A review and outlook, Sci. Total Environ., 574, 332–349, https://doi.org/10.1016/j.scitotenv.2016.09.040, 2017.

Xu, W., Han, T., Du, W., Wang, Q., Chen, C., Zhao, J., Zhang, Y., Li, J., Fu, P., Wang, Z., Worsnop, D. R., and Sun, Y.: Effects of Aqueous-Phase and Photochemical Processing on Secondary Organic Aerosol Formation and Evolution in Beijing, China, Environ. Sci. Technol., 51, 762–770, https://doi.org/10.1021/acs.est.6b04498, 2017.

Yinhui, W., Rong, Z., Yanhong, Q., Jianfei, P., Mengren, L., Jianrong, L., Yusheng, W., Min, H., and Shijin, S.: The impact of fuel compositions on the particulate emissions of direct injection gasoline engine, Fuel, 166, 543–552, https://doi.org/10.1016/j.fuel.2015.11.019, 2016.

Yu, Y., Wang, H., Wang, T., Song, K., Tan, T., Wan, Z., Gao, Y., Dong, H., Chen, S., Zeng, L., Hu, M., Wang, H., Lou, S., Zhu, W., and Guo, S.: Elucidating the importance of semi-volatile organic compounds to secondary organic aerosol formation at a regional site during the EXPLORE-YRD campaign, Atmos. Environ., 246, 118043, https://doi.org/10.1016/j.atmosenv.2020.118043, 2020.

Zhan, J., Feng, Z., Liu, P., He, X., He, Z., Chen, T., Wang, Y., He, H., Mu, Y., and Liu, Y.: Ozone and SOA formation potential based on photochemical loss of VOCs during the Beijing summer, Environ. Pollut., 285, 117444, https://doi.org/10.1016/j.envpol.2021.117444, 2021.

Zhang, Q., Worsnop, D. R., Canagaratna, M. R., and Jimenez, J. L.: Hydrocarbon-like and oxygenated organic aerosols in Pittsburgh: insights into sources and processes of organic aerosols, Atmos. Chem. Phys., 5, 3289–3311, https://doi.org/10.5194/acp-5-3289-2005, 2005.

Zhang, Q., Jimenez, J. L., Canagaratna, M. R., Ulbrich, I. M., Ng, N. L., Worsnop, D. R., and Sun, Y.: Understanding atmospheric organic aerosols via factor analysis of aerosol mass spectrometry: a review, Anal. Bioanal. Chem., 401, 3045–3067, https://doi.org/10.1007/s00216-011-5355-y, 2011.

Zhang, R., Wang, G., Guo, S., Zamora, M. L., Ying, Q., Lin, Y., Wang, W., Hu, M., and Wang, Y.: Formation of urban fine particulate matter, Chem. Rev., 115, 3803–3855, https://doi.org/10.1021/acs.chemrev.5b00067, 2015.

Zhang, Y., Deng, W., Hu, Q., Wu, Z., Yang, W., Zhang, H., Wang, Z., Fang, Z., Zhu, M., Li, S., Song, W., Ding, X., and Wang, X.: Comparison between idling and cruising gasoline vehicles in primary emissions and secondary organic aerosol formation during photochemical ageing, Sci. Total Environ., 722, 137934, https://doi.org/10.1016/j.scitotenv.2020.137934, 2020a.

Zhang, Z., Zhu, W., Hu, M., Wang, H., Chen, Z., Shen, R., Yu, Y., Tan, R., and Guo, S.: Secondary Organic Aerosol from Typical Chinese Domestic Cooking Emissions, Environ. Sci. Tech. Let., 8, 24–31, https://doi.org/10.1021/acs.estlett.0c00754, 2020b.

Zhang, Z., Hu, M., et al.: Secondary Organic Aerosol Formation from Urban Lifestyle Sources in Beijing, in preparation, 2021.

Zhao, Y., Nguyen, N. T., Presto, A. A., Hennigan, C. J., May, A. A., and Robinson, A. L.: Intermediate Volatility Organic Compound Emissions from On-Road Diesel Vehicles: Chemical Composition, Emission Factors, and Estimated Secondary Organic Aerosol Production, Environ. Sci. Technol., 49, 11516–11526, https://doi.org/10.1021/acs.est.5b02841, 2015.

Zhao, Y., Lambe, A. T., Saleh, R., Saliba, G., and Robinson, A. L.: Secondary Organic Aerosol Production from Gasoline Vehicle Exhaust: Effects of Engine Technology, Cold Start, and Emission Certification Standard, Environ. Sci. Technol., 52, 1253–1261, https://doi.org/10.1021/acs.est.7b05045, 2018.

Zhao, Y. L., Saleh, R., Saliba, G., Presto, A. A., Gordon, T. D., Drozd, G. T., Goldstein, A. H., Donahue, N. M., and Robinson, A. L.: Reducing secondary organic aerosol formation from gasoline vehicle exhaust, P. Natl. Acad. Sci. USA, 114, 6984–6989, https://doi.org/10.1073/pnas.1620911114, 2017.

Zhong, L. J., Goldberg, M. S., Gao, Y. T., and Jin, F.: Lung cancer and indoor air pollution arising from Chinese style cooking among nonsmoking women living in Shanghai, China, Epidemiology, 10, 488–494, https://doi.org/10.1097/00001648-199909000-00005, 1999.

Zhou, W., Xu, W., Kim, H., Zhang, Q., Fu, P., Worsnop, D. R., and Sun, Y.: A review of aerosol chemistry in Asia: insights from aerosol mass spectrometer measurements, Environ. Sci., 22, 1616–1653, https://doi.org/10.1039/d0em00212g, 2020.